Robust In-situ Adaptive Artificial Interface for Dead-lithium-free Lithium Metal Batteries

Chengkai Yang[a,*], Jing Luo[a], Jiajie Wu[a], Borong Li[a], Yichen Li[a], Dehuan Shi[a], Yanbin Qiu[a], Xinyu Zheng[a],Qian Wang[d,*], Zheyuan Liu[a,*],Shuming Duan[b,c*]

a Key Laboratory of Advanced Materials Technologies, International (Hong Kong Macao and Taiwan) Joint Laboratory on Advanced Materials Technologies, College of Materials Science and Engineering, Fuzhou University, Fuzhou, Fujian, 350108, China
b Joint School of National University of Singapore and Tianjin University, International Campus of Tianjin University, Binhai New City, Fuzhou, 350207, China
c Key Laboratory of Organic Integrated Circuits, Ministry of Education, Tianjin Key Laboratory of Molecular Optoelectronic Sciences, Tianjin University, Tianjin, 300072, China.
d College of Materials Science and Engineering, Taiyuan University of Technology, Taiyuan, Shanxi 030024, China
E-mail: chengkai_yang@fzu.edu.cn; qianwang0825@pku.edu.cn; zheyuan.liu@fzu.edu.cn; smduan@tjufz.org.cn

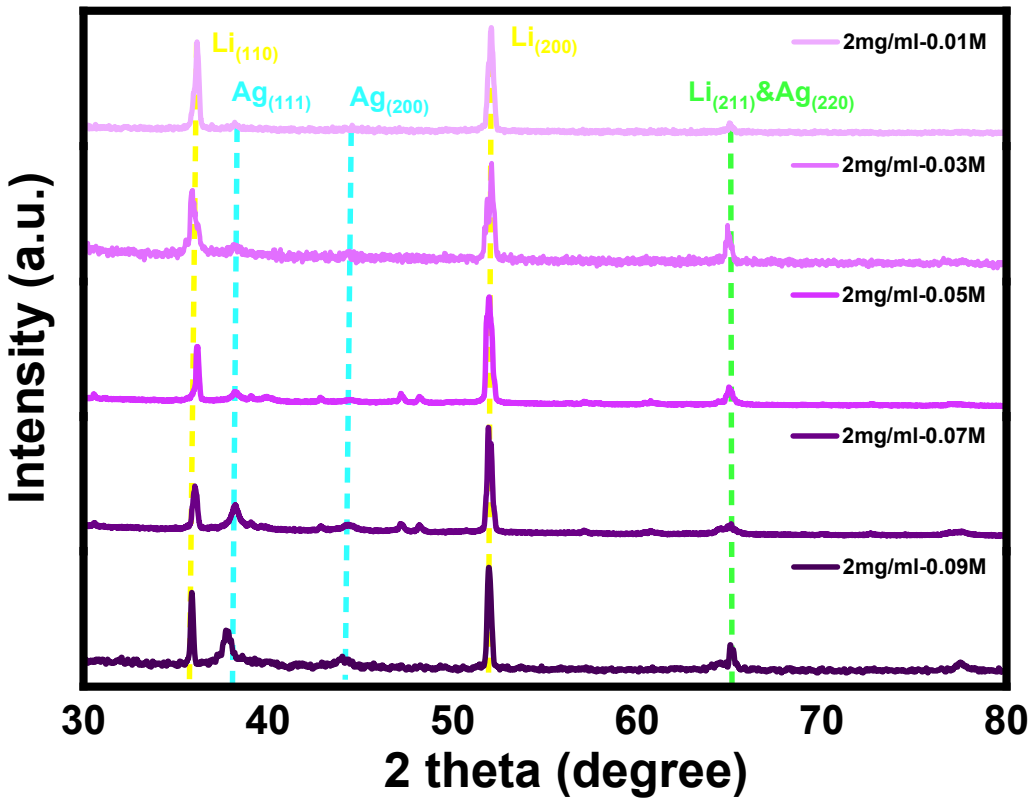

Fig.S1 XRD patterns of PAM-b-PHFBA-$AgNO_3$@Li prepared at different concentrations.

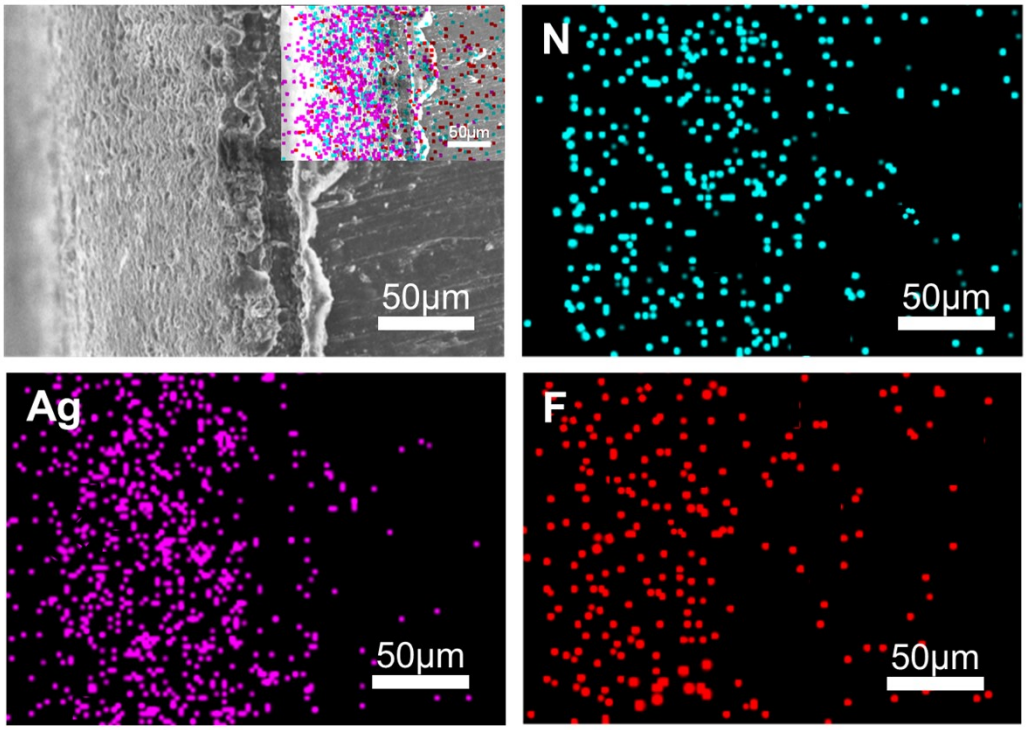

Fig.S2 EDS spectrum of the cross-section of PAM-b-PHFBA-$AgNO_3$@Li (including N, Ag, and F).

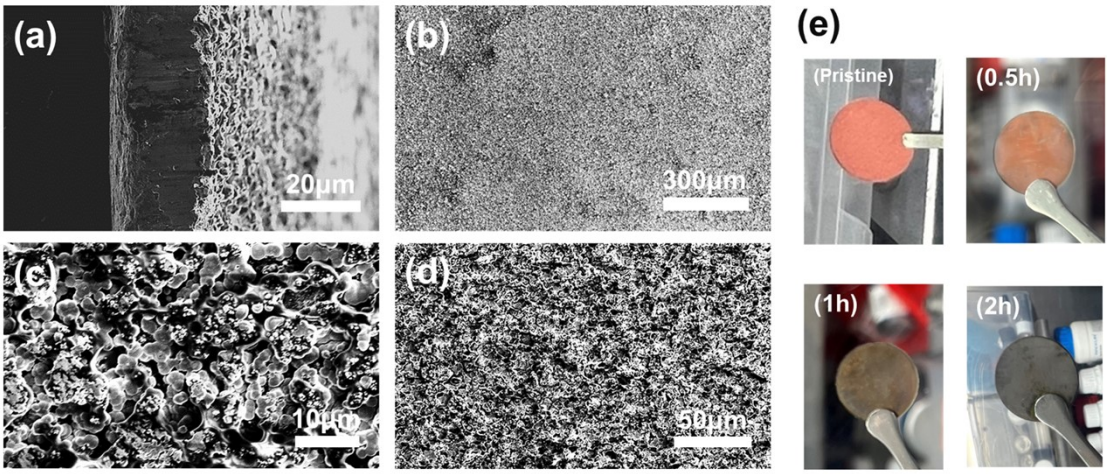

Fig.S3 (a) Cross-sectional view and (b) top view of PAM-b-PHFBA-$AgNO_3$@Cu. (d) Magnified view of (b). (c) Magnified view of (d). (e) Optical micrographs after different in situ reaction times.

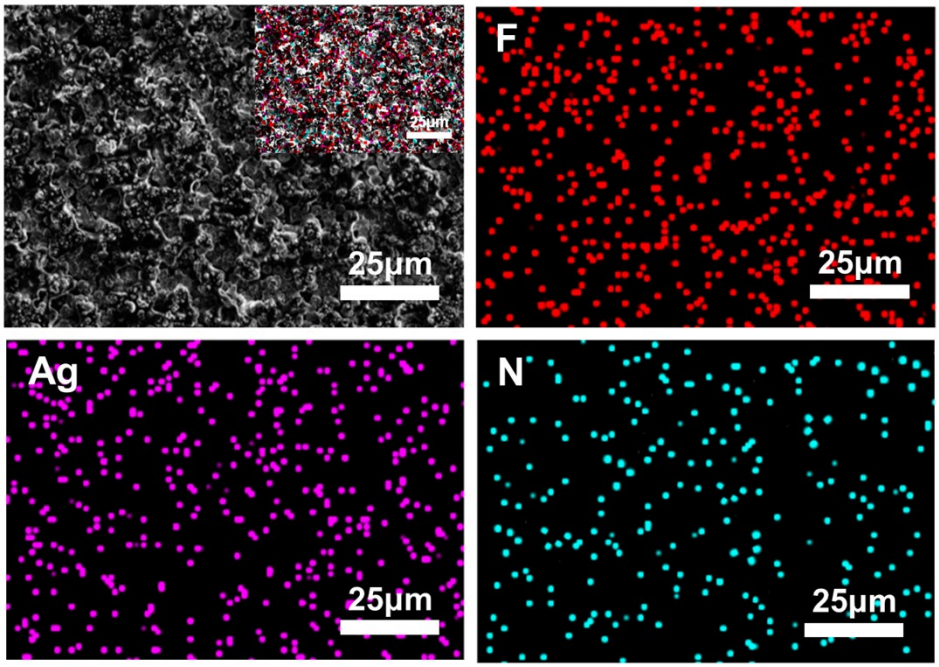

Fig.S4 EDS spectrum of the surface of PAM-b-PHFBA-$AgNO_3$@Cu (including N, Ag, and F).

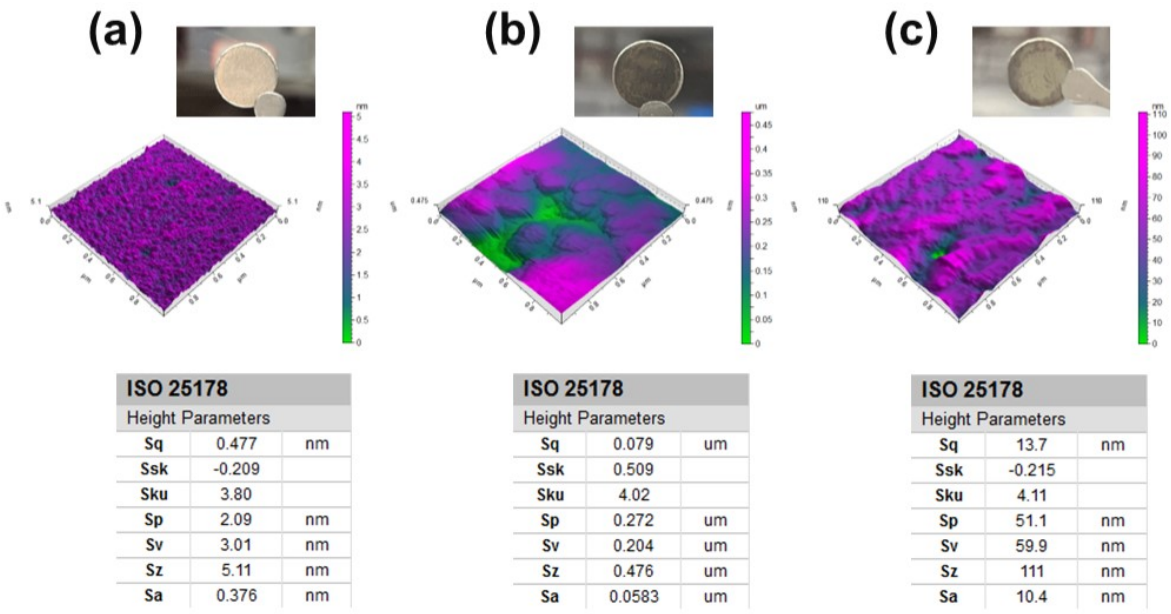

ISO 25178		
Height Parameters		
Sq	0.477	nm
Ssk	-0.209	
Sku	3.80	
Sp	2.09	nm
Sv	3.01	nm
Sz	5.11	nm
Sa	0.376	nm

ISO 25178		
Height Parameters		
Sq	0.079	um
Ssk	0.509	
Sku	4.02	
Sp	0.272	um
Sv	0.204	um
Sz	0.476	um
Sa	0.0583	um

ISO 25178		
Height Parameters		
Sq	13.7	nm
Ssk	-0.215	
Sku	4.11	
Sp	51.1	nm
Sv	59.9	nm
Sz	111	nm
Sa	10.4	nm

Fig. S5 Three-dimensional AFM morphology and surface information of (a) PAM-b-PHFBA@Li, (b) $AgNO_3$@Li, and (c) PAM-b-PHFBA-$AgNO_3$@Li.

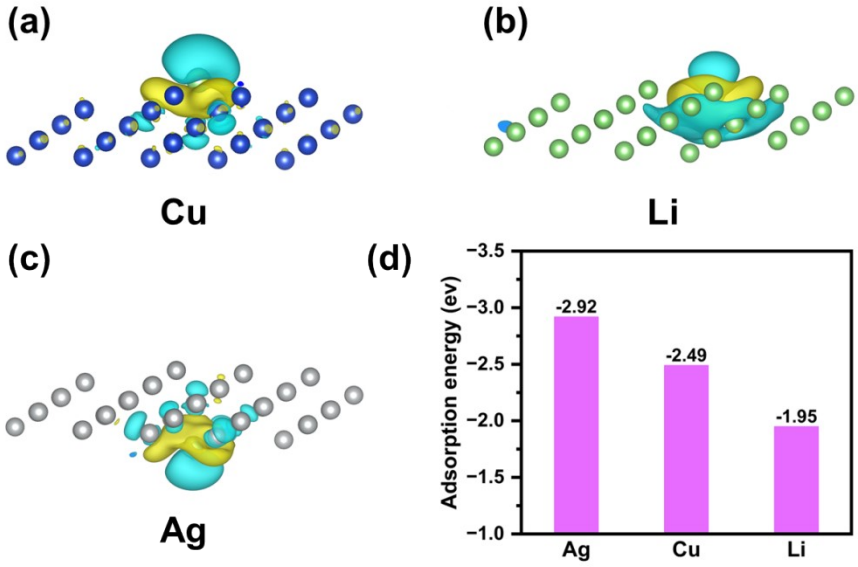

Fig. S6 (a) Charge density difference maps of lithium atoms adsorbed on (a) Cu, (b) Li, and (c) Ag substrates. (d) Adsorption energy diagram.

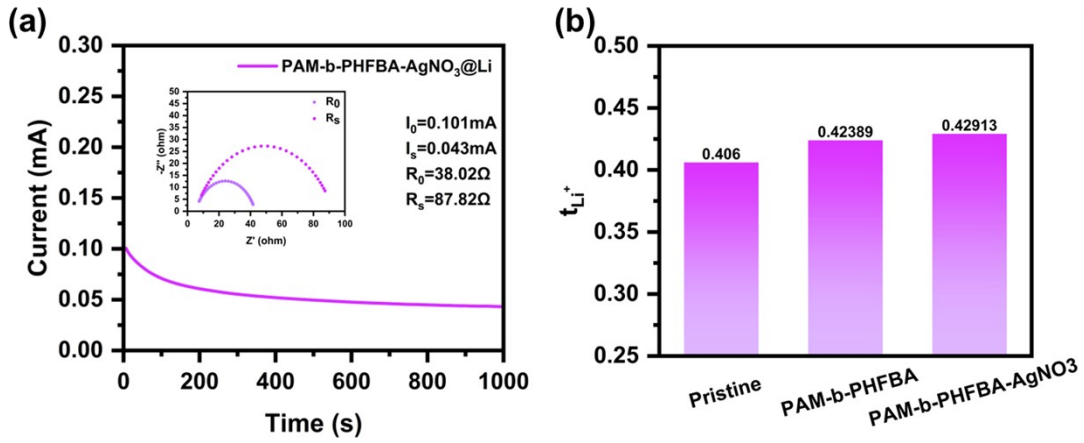

Fig. S7 (a) lithium ion migration number test. (b) Lithium ion migration numbers calculated from the test.

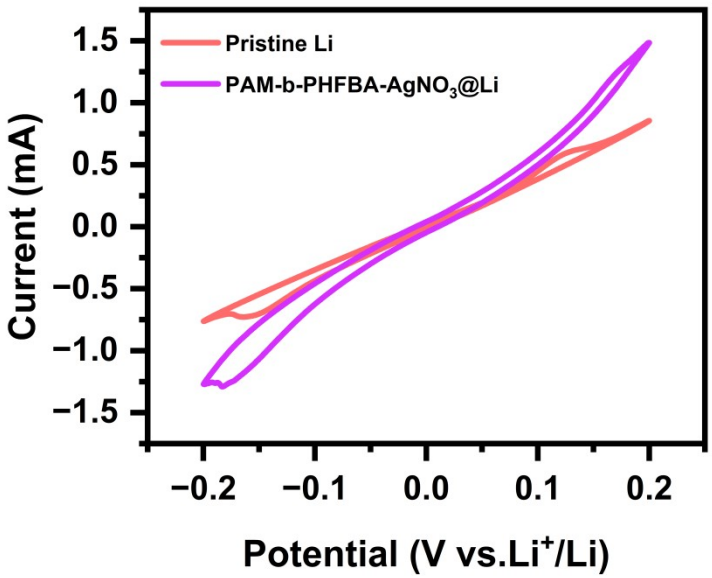

Fig. S8. CV curves of symmetric cells assembled with Pristine Li and PAM-b-PHFBA-$AgNO_3$@Li.

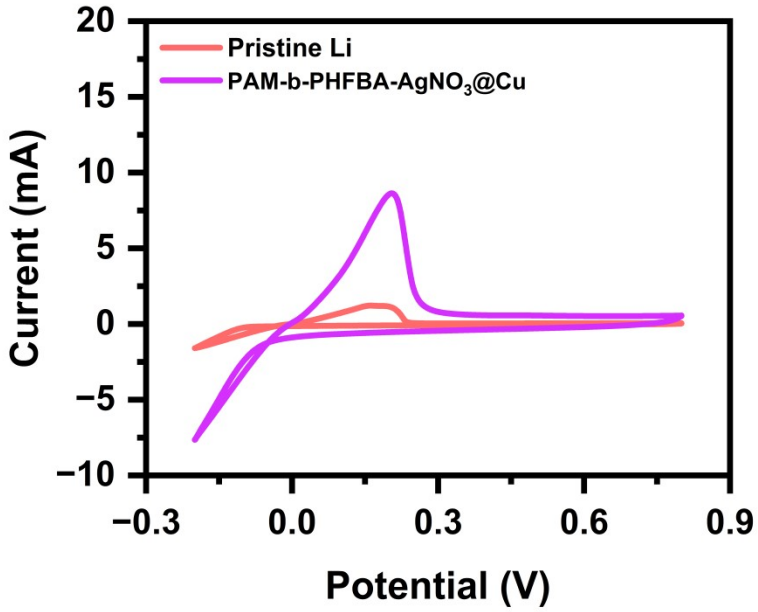

Fig. S9 CV curves of symmetric cells assembled with Pristine Cu and PAM-b-PHFBA-$AgNO_3$@Cu.

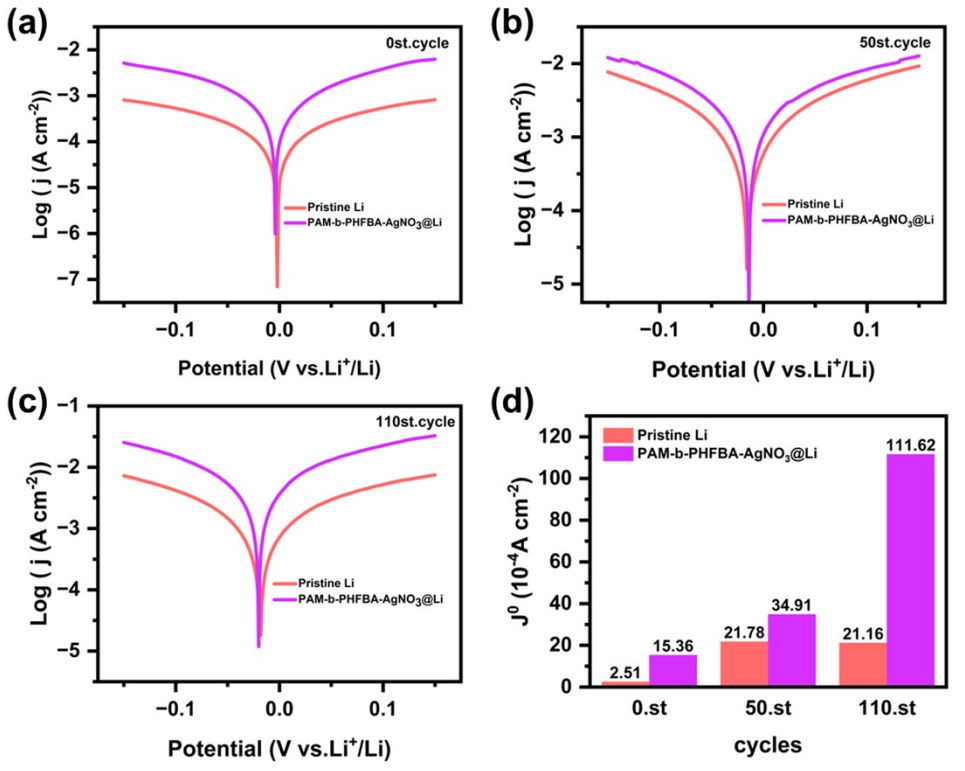

Fig. S10 Tafel plots after cycling of the battery for (a) 0, (b) 50, and (c) 110 cycles. (d) Comparison of exchange current densities.

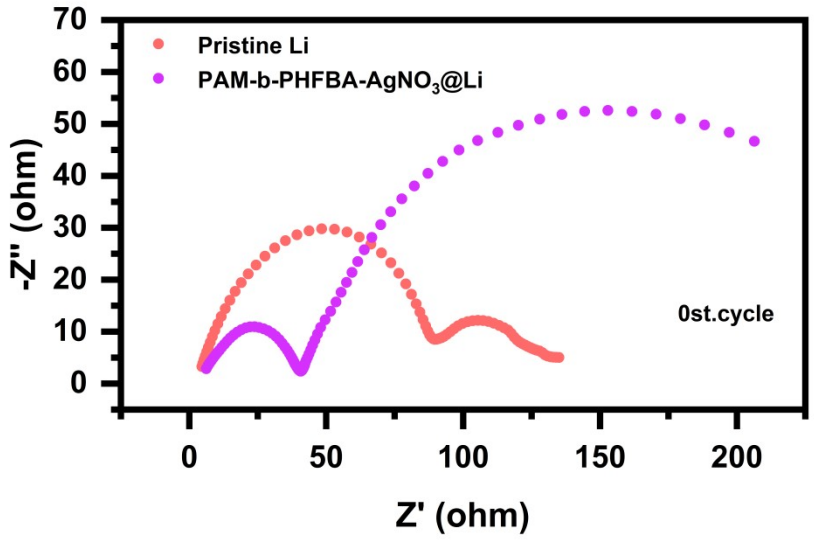

Fig. S11 Impedance spectra of symmetric cells assembled with Pristine Li and PAM-b-PHFBA-$AgNO_3$@Li before cycling.

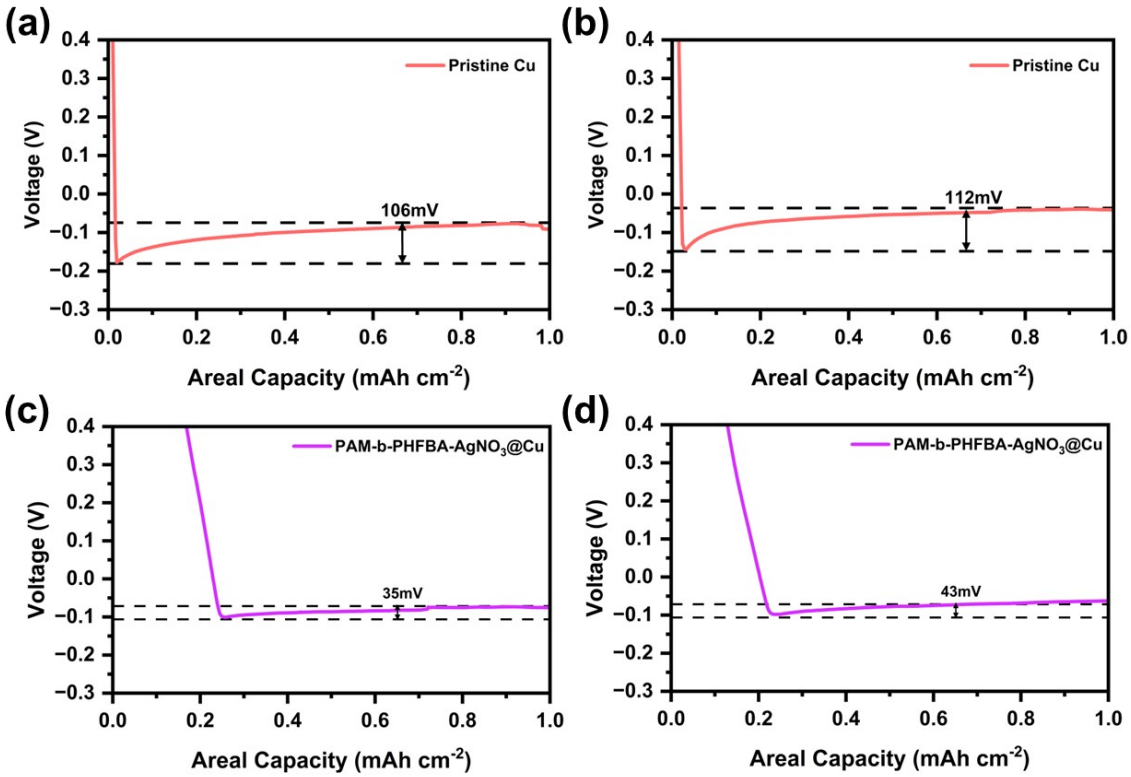

Fig. S12 Nucleation overpotential of Pristine Li at (a) 0.5 mA cm^{-2} and (b) 1 mA cm^{-2}. Nucleation overpotential of PAM-b-PHFBA-$AgNO_3$@Cu at (c) 0.5 mA cm^{-2} and (d) 1 mA cm^{-2}.

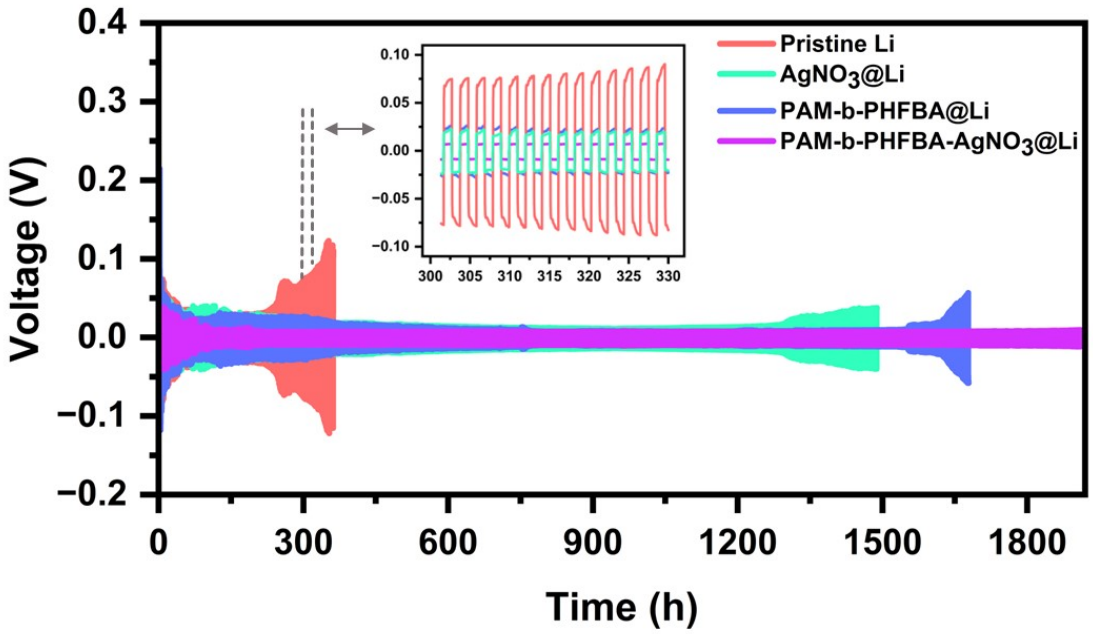

Fig. S13 Voltage distribution of Li||Li symmetric cells with Pristine Li, $AgNO_3$@Li, PAM-b-PHFBA@Li, and PAM-b-PHFBA-$AgNO_3$@Li at a current density of 1 mA cm^{-2} with a capacity of 1 mAh cm^{-2}.

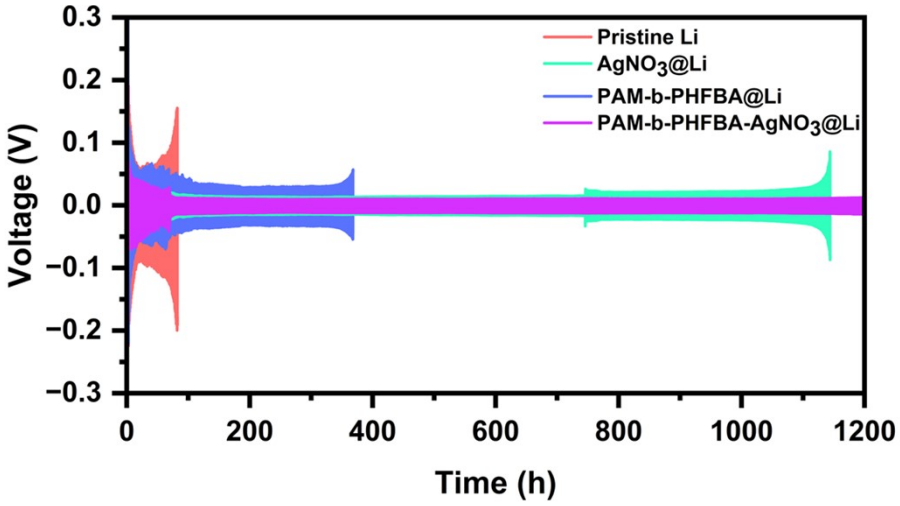

Fig. S14 Voltage distribution of Li||Li symmetric cells with Pristine Li, $AgNO_3$@Li, PAM-b-PHFBA@Li, and PAM-b-PHFBA-$AgNO_3$@Li at a current density of 3 mA cm^{-2} with a capacity of 1 mAh cm^{-2}.

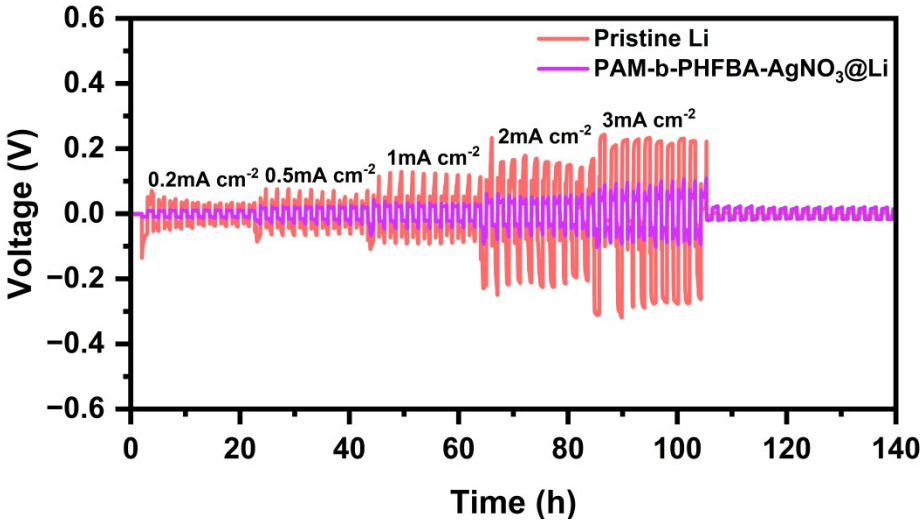

Fig. S15 Stepwise current test of Pristine Li and PAM-b-PHFBA-$AgNO_3$@Li.

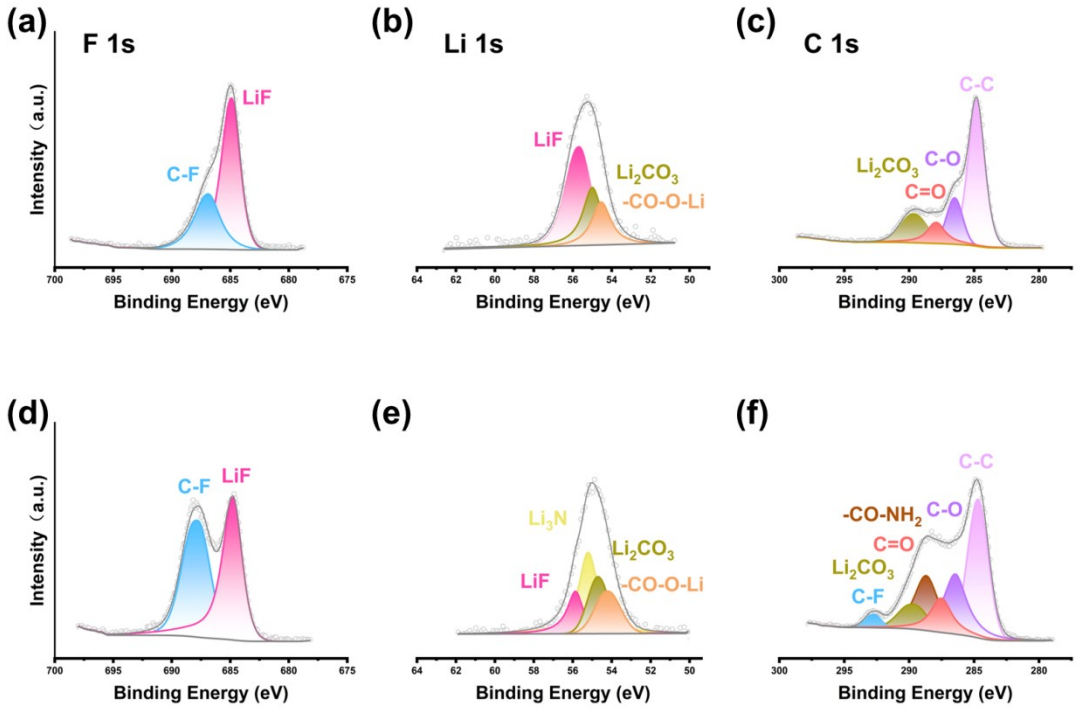

Fig. S16 F 1s, Li 1s, and C 1s XPS spectra of Li||Li symmetric cells assembled with (a-c) Pristine Li and (d-f) PAM-b-PHFBA-$AgNO_3$@Li after 50 cycles at 1 mA cm^{-2}/1 mAh cm^{-2}.

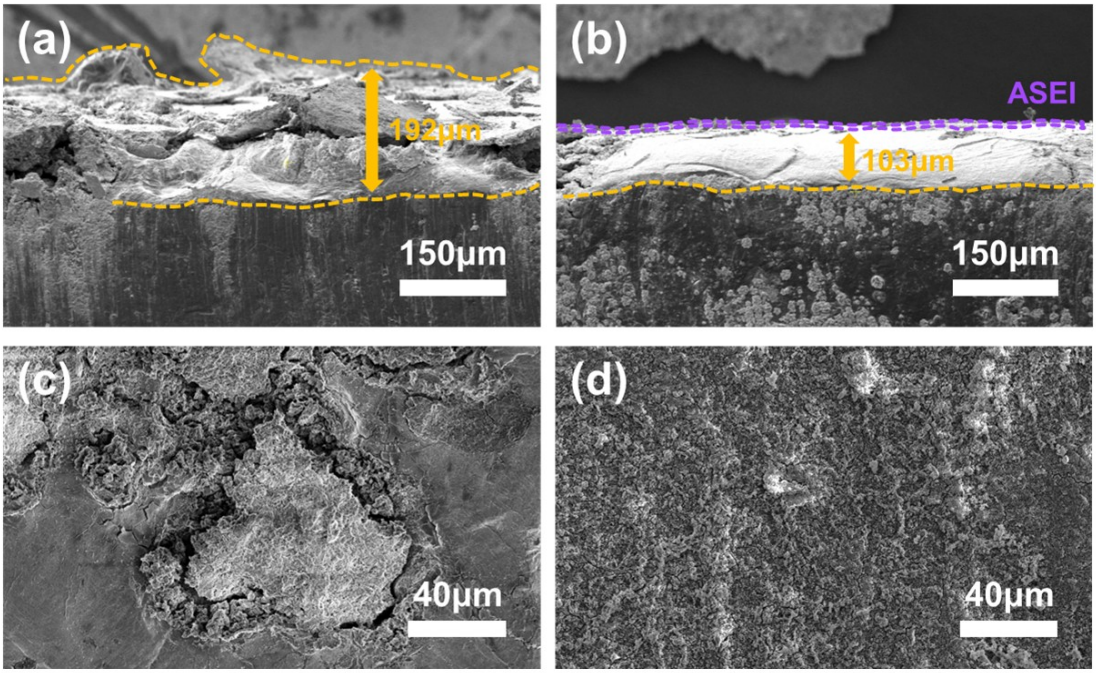

Fig. S17 Cross-sectional views of (a) Pristine Li and (b) PAM-b-PHFBA-$AgNO_3$@Li after 50 cycles at 3 mA cm^{-2}. Top views of (c) Pristine Li and (d) PAM-b-PHFBA-$AgNO_3$@Li after 50 cycles at 3 mA cm^{-2}.

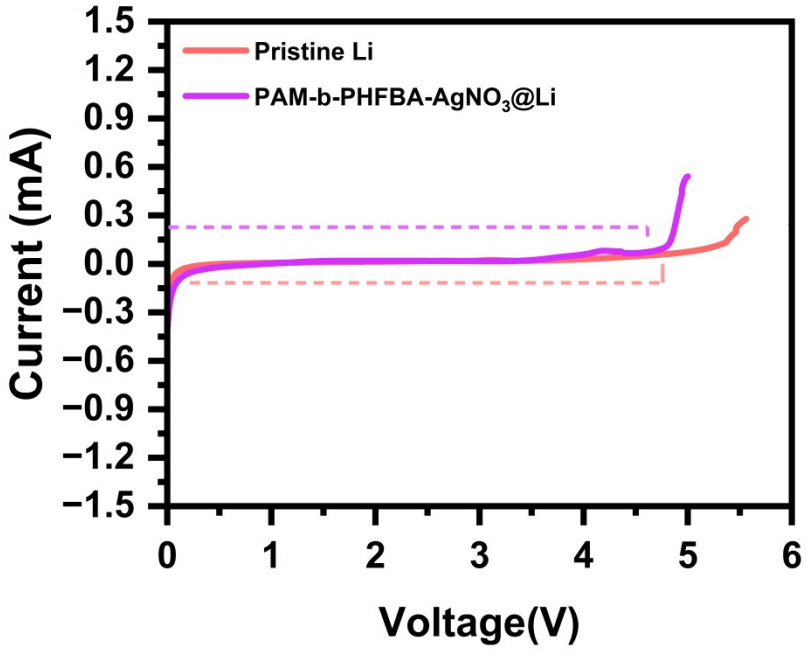

Fig. S18 Linear sweep voltammetry (LSV) positive scan current curves.

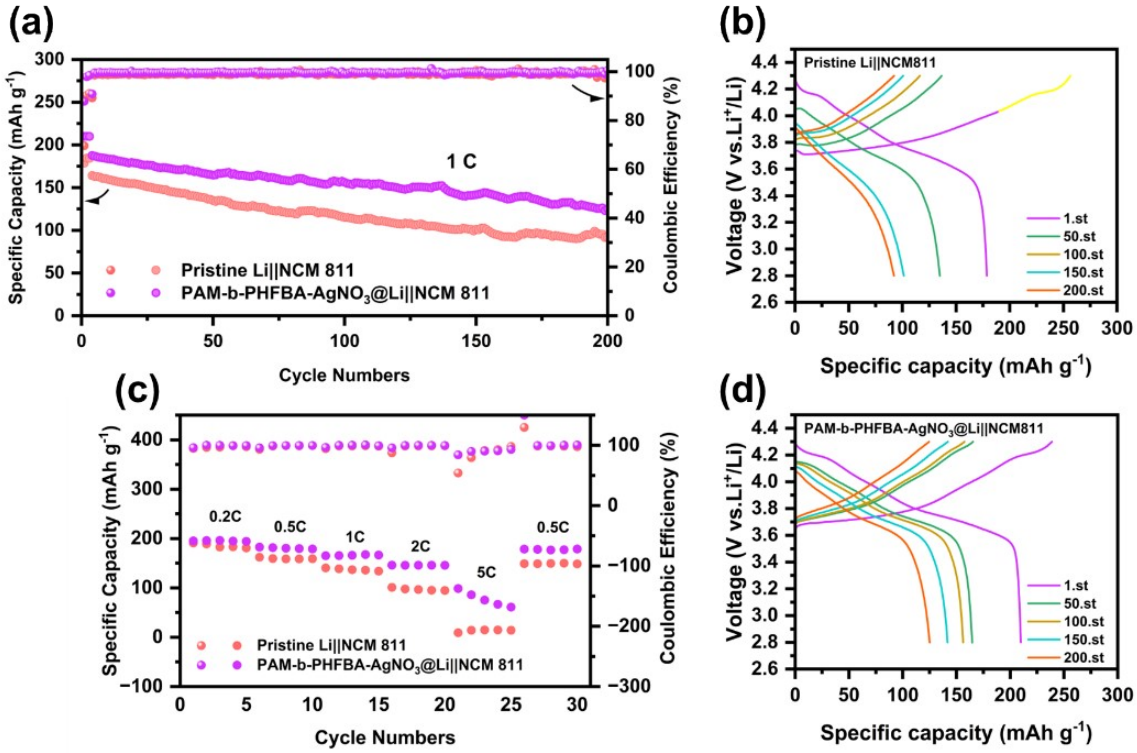

Fig. S19 (a) Cycling performance of the ternary full cells assembled with Pristine Li and PAM-b-PHFBA-$AgNO_3$@Li at 1 C. (c) Rate performance test. (b) Voltage-capacity curves of the full cells with Pristine Li and (d) PAM-b-PHFBA-$AgNO_3$@Li.

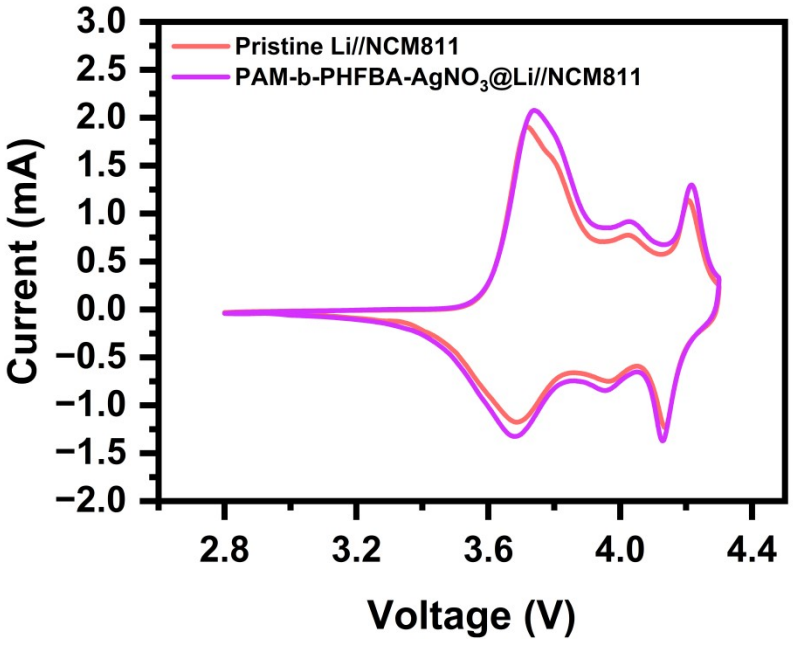

Fig. S20 CV curves of the ternary full cells assembled with Pristine Li and PAM-b-PHFBA-$AgNO_3$@Li.

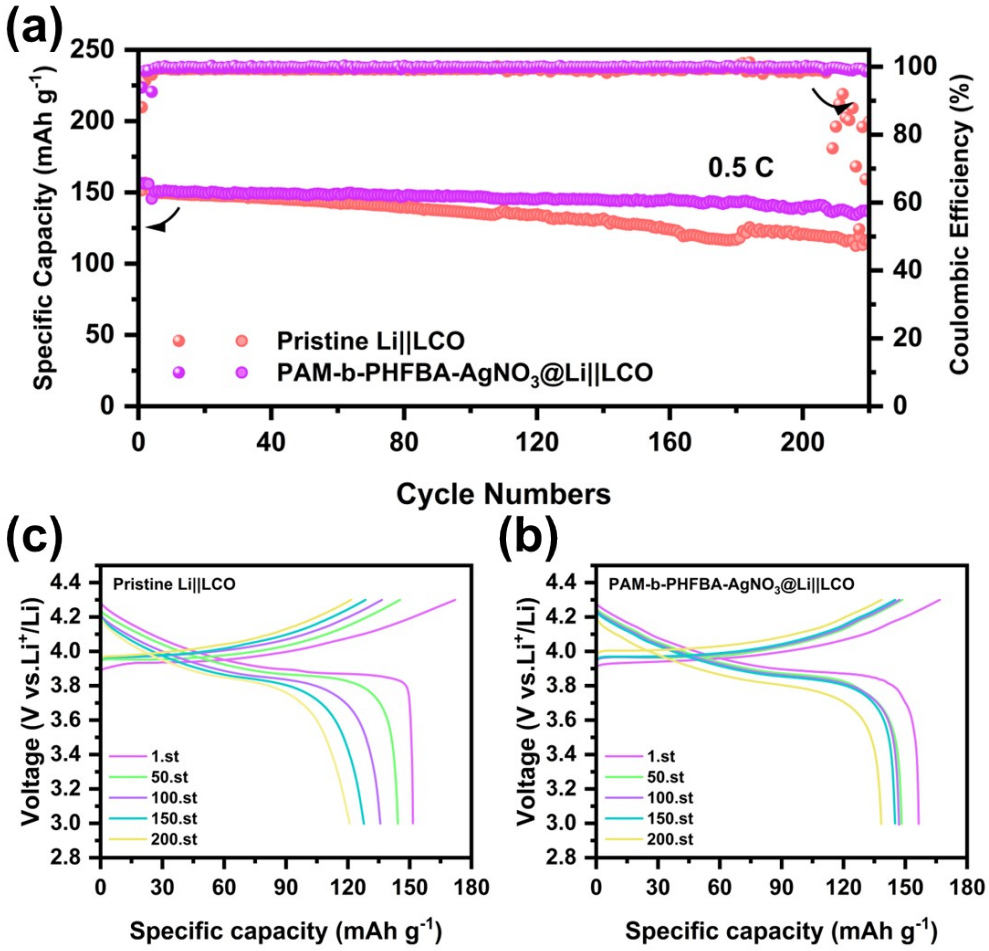

Fig. S21 (a) Cycling performance at 0.5 C of lithium cobalt oxide full cells assembled with Pristine Li and PAM-b-PHFBA-$AgNO_3$@Li. (b) Voltage-capacity curves of full cells with Pristine Li and (c) PAM-b-PHFBA-$AgNO_3$@Li.

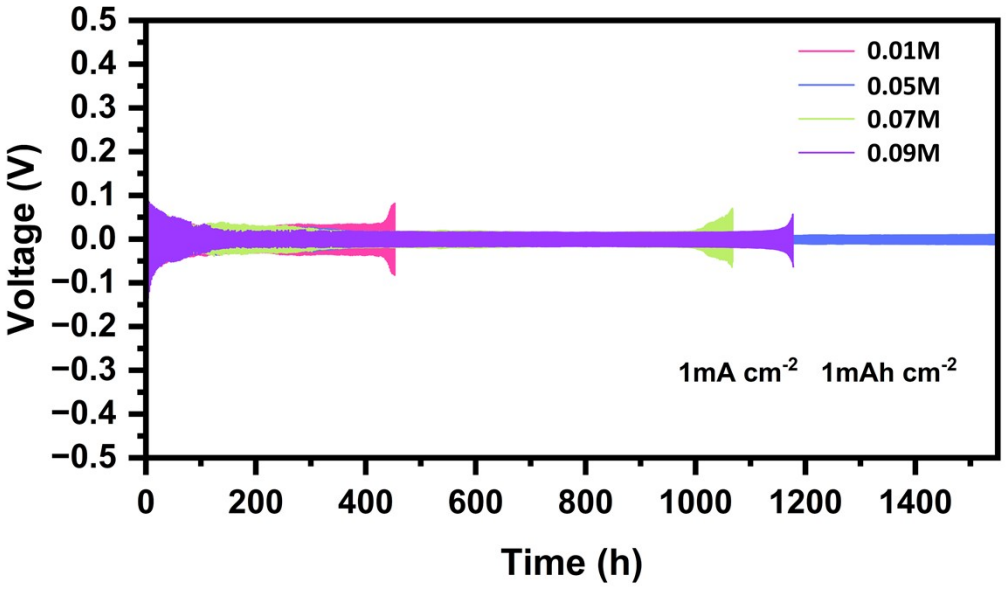

Fig. S22 Cycling images of lithium symmetric cells assembled with PAM-b-PHFBA-$AgNO_3$ (prepared using silver nitrate at concentrations of 0.01, 0.05, 0.07, and 0.09 M)

Fig. S23. Cross-sectional and top-view SEM images of Li anodes after 50 cycles at 3 mA cm^{-2}. Cross-sectional views of (a) Pristine Li and (b) PAM-b-PHFBA-$AgNO_3$@Li; Top views of (c) Pristine Li and (d) PAM-b-PHFBA-$AgNO_3$@Li. The Pristine Li anode shows severe dendrite growth and structural damage, while the composite-coated Li anode maintains a compact and intact structure, confirming the dendrite suppression effect of the in-situ adaptive ASEI

Table 1 Performance comparison between this work and recent interface modifications (2017 – 2025).

Reference(DOI)	Title	Battery performance	Year
(10.1149/1945-7111/aa8d12)	Altering the Solid Electrolyte Interface Through Surface-Modification of Lithium Metal Anode for High-Voltage Lithium Battery	NMC622/Li full cell: ~141 mAh g^{-1} after 100 cycles; Li/Li symmetrical cell: stable plating/stripping over 450 h at 0.5 mA cm^{-2}; Improved capacity retention and rate capability via optimized	2024

		organic/inorganic SEI.	
(10.1016/j.jechem.2022.02.041)	Bifunctional LiI additive for poly(ethylene oxide) electrolyte with high ionic conductivity and stable interfacial chemistry	Ionic conductivity: 2.1×10^{-4} S cm^{-1} at 45° C; Li/Li symmetrical cell: stable cycling >600 h at 0.2 mA cm^{-2}; Solid-state LFP/Li and NCM811/Li cells show excellent cycling stability and rate performance.	2022
(10.1016/j.matchemphys.2023.128177)	Surface modification of lithium metal anode with lithium silicate-lithium phosphate composite layer for enhanced cycling stability	Li/Li symmetrical cell: stable for 500 h at 1 mA cm^{-2}; LFP/Li full cell: good cycling stability over 300 cycles at 1C; Enhanced Li^+ conductivity and mechanical strength suppress dendrite growth.	2023
(10.1002/anie.201709305)	Lithium Azide as an Electrolyte Additive for All-Solid-State Lithium–Sulfur Batteries	Li/Li symmetrical cell: >2000 h cycling at 0.1 mA cm^{-2}; All-solid-state Li–S cell: high reversible capacity (~800 mAh g^{-1}) and improved capacity retention over 30 cycles at 70° C; Li_3N-rich SEI enhances interfacial stability.	2017
This study	/	3 mA cm^{-2}/1 mAh cm^{-2}: Cycling for >1200 h; NCM811 high-nickel cathode	